ISSN 1063-7788, Physics of Atomic Nuclei, 2017, Vol. 80, No. 9, pp. 1549–1552. © Pleiades Publishing, Ltd., 2017.
Original Russian Text © S.A. Bulychev, A.E. Kudryavtsev, V.V. Kulikov, M.A. Martem'yanov, V.E. Tarasov, W.J. Briscoe, I.I. Strakovsky, 2016, published in Yadernaya Fizika i Inzhiniring, 2016, Vol. 7, No. 4, pp. 374–378.

INTERACTION OF PLASMA, PARTICLE BEAMS, AND RADIATION WITH MATTER

Neutral Pion Photoproduction on Neutron

S. A. Bulychev[a], A. E. Kudryavtsev[a], V. V. Kulikov[a], M. A. Martem'yanov[a,*], V. E. Tarasov[a], W. J. Briscoe[b], and I. I. Strakovsky[b]

[a] *Alikhanov Institute of Theoretical and Experimental Physics, National Research Center Kurchatov Institute, Moscow, 117218 Russia*

[b] *George Washington University, Washington, DC 20052, USA*

**e-mail: mmartemi@gmail.com*

Received November 16, 2016

Abstract—The reaction $\gamma n \to \pi^0 n$ is investigated both theoretically and experimentally as an important step toward determining the electromagnetic coupling constants of the N^* and Δ^* resonances [1]. We analyze the data on the collisions of γ quanta with energies between 200 and 800 MeV with a deuterium target collected by the A2 experiment in Mainz, Germany. These complement the data for neutral-pion photoproduction on protons obtained by the same experiment [2].

Keywords: A2 experiment, pion photoproduction, Crystal Ball, deuterium target, total and differential cross sections

DOI: 10.1134/S1063778817090022

1. INTRODUCTION

Investigating the electromagnetic properties of nucleon resonances in the processes of meson photoproduction is one of the topical issues of particle physics. Though a large amount of experimental data has been collected for pion photoproduction on protons, such reactions as $\gamma n \to \pi^0 n$ and $\gamma n \to \pi^- p$ have not been measured since neutron targets were not available. However, a combined analysis of photoproduction data for both proton and neutron targets is required for fully determining the electromagnetic coupling constants of the Δ^* and N^* resonances and probing the isospin structure of the production amplitudes. The process of pion photoproduction on a neutron can be experimentally assessed by using deuterium as a target. Within this approach, significant effects of final-state interactions (FSI) should be taken into account when extracting the reaction $\gamma N \to \pi^0 N$ from the detected $\gamma d \to \pi^0 NN$ collisions. A detailed description of the FSI effect can be found in [3–5].

2. A2 DETECTOR

The analyzed data were collected by exposing the A2 detector to a tagged-photon beam with energy up to 800 MeV in March 2013. The beam impinged on a cylindrical deuterium target with length of 10 cm and diameter of 4 cm deployed in the central part of the detector. The broad-aperture detecting system schematically shown in Fig. 1 is formed by the Crystal Ball (CB) calorimeter, the TAPS spectrometer, a cylindrical scintillation detector for secondary-particle identification (PID), and a multiwire proportional chamber (MWPC). The spherical CB calorimeter comprises 672 optically isolated NaI(TI) crystals and subtends the emission polar-angle region between 20° and 160°, covering some 93% of the full solid angle [6, 7]. The CB sphere features inlet and outlet windows for transporting the beam and an internal cavity with radius of 25 cm for deploying the target and the nearby detecting elements. The calorimeter is tuned so as to efficiently detect both the charged secondaries and photons. Apart from that, the CB calorimeter proved to be capable of detecting secondary neutrons over a broad energy range. Charged secondaries are identified by ionization losses using the PID detector, which consists of 24 scintillator plates [8].

3. SELECTING THE REACTION OF PION PHOTOPRODUCTION

The reaction $\gamma n \to \pi^0 n$ is selected by requiring that all final-state particles be detected in the CB calorimeter, producing three clusters. The neutral pion is selected as a photon pair with effective mass $m_{\gamma\gamma}$ closest to the nominal pion mass. When selecting the neutron-induced cluster in the calorimeter, one has to reject the background events due to the reaction $\gamma p \to \pi^0 p$. The energetic charged component is detected using the PID scintillator array, and such events are rejected at the analysis stage. The kinematics of the process $\gamma d \to \pi^0 np$ are fully determined by the reconstructed neutral pion and the position of the addi-

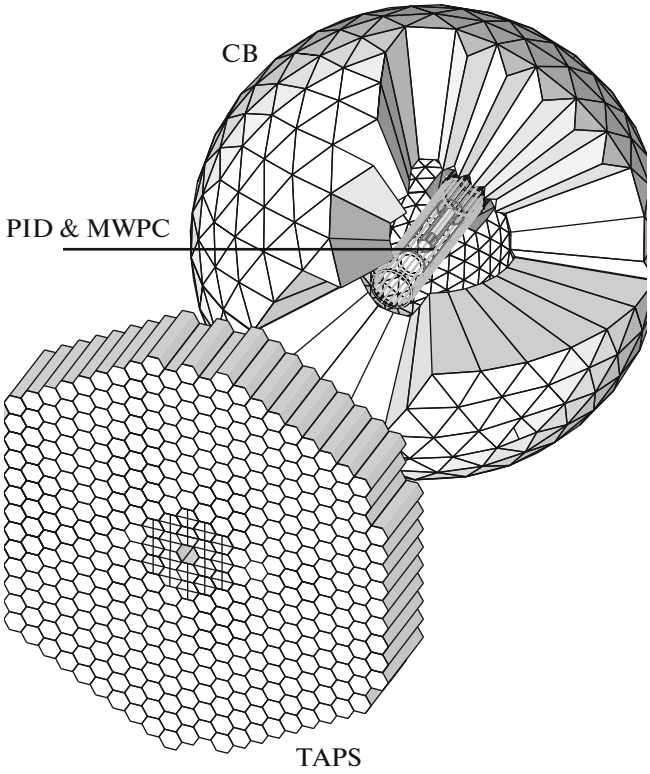

Fig. 1. Layout of the A2 detector.

tional cluster from which the neutron's direction of motion is inferred. By analyzing the shape of the proton momentum spectrum, one is able to reject the background events involving the emission of two neutral pions. The detection efficiency for the investigated reaction is computed through a simulation based on the GEANT4 program package. The simulation relies on the neutron detection efficiency as extracted from the experimental data [9].

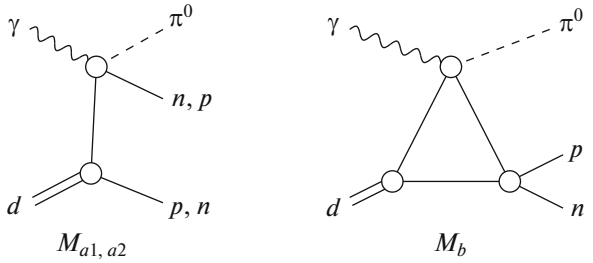

Fig. 2. Impulse-approximation (M_{a1}, M_{a2}) and *NN*-FSI (M_b) diagrams for the reaction $\gamma d \to \pi^0 np$.

4. EXTRACTING THE TOTAL AND DIFFERENTIAL CROSS SECTIONS

To accurately compute the total and differential cross sections of the discussed reaction, a model formalism for the reaction $\gamma d \to \pi NN$ was developed in [5] which takes into account the effects of the *NN* and πN final-state interactions in addition to the contributions of the impulse-approximation (IA) diagrams. The input data for the formalism are the phenomenological amplitudes of the $\gamma N \to \pi N$ reaction and the *NN* and πN interactions taken from the SAID partial-wave analysis [10]. The deuteron wave function is substituted in the Bonn potential form [11]. In this analysis, a simplified version of the formalism [5] is employed in order to reduce the volume of computations. Namely, here we neglect the effects of the final-state interaction πN-FSI which are important near the reaction threshold but are small for photon energies of $E_\gamma > 200$ MeV [4]. The *NN*-FSI effect, which is significant near the *NN* threshold, is taken into account only for the *s* wave, where its contribution is dominant. Then, the amplitude *M* of the reaction $\gamma d \to \pi^0 np$ has the form

$$M = M_{a1} + \Delta, \quad \Delta = M_{a2} + M_b, \tag{1}$$

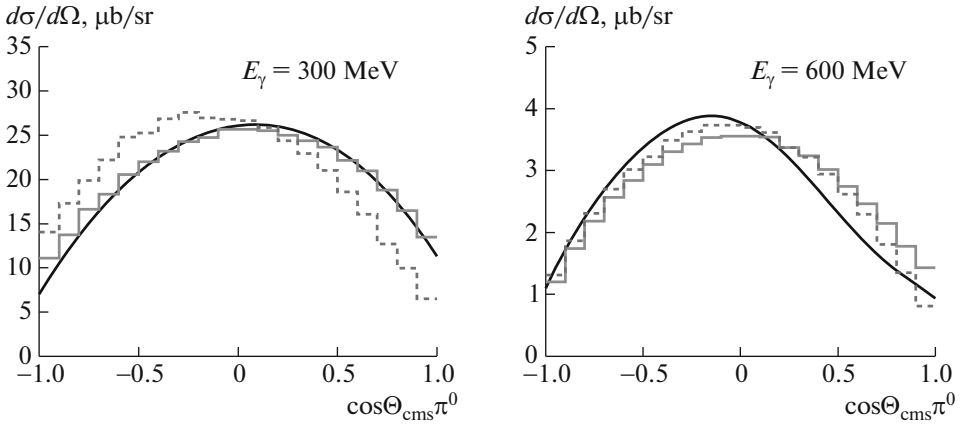

Fig. 3. Calculated $\gamma n \to \pi^0 n$ differential cross section as a function of the cosine of the π^0 emission angle in cms for incident-photon energies of 300 and 600 MeV. The cross sections obtained with and without taking into account the FSI effect are depicted by dashed curves and histograms, respectively. The SAID predictions are shown by solid curves.

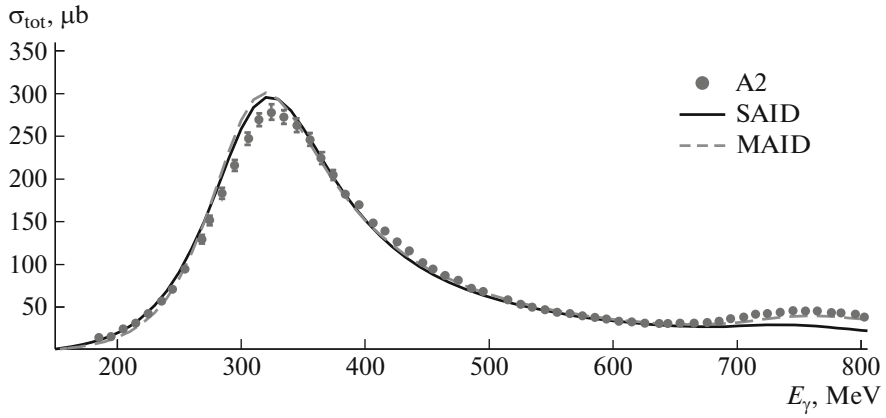

Fig. 4. Total $\gamma n \to \pi^0 n$ cross section as a function of incident-photon energy. Our preliminary measurements are depicted by points with error bars. The results of the SAID and MAID partial-wave analyses are shown by the solid and dashed curves, respectively.

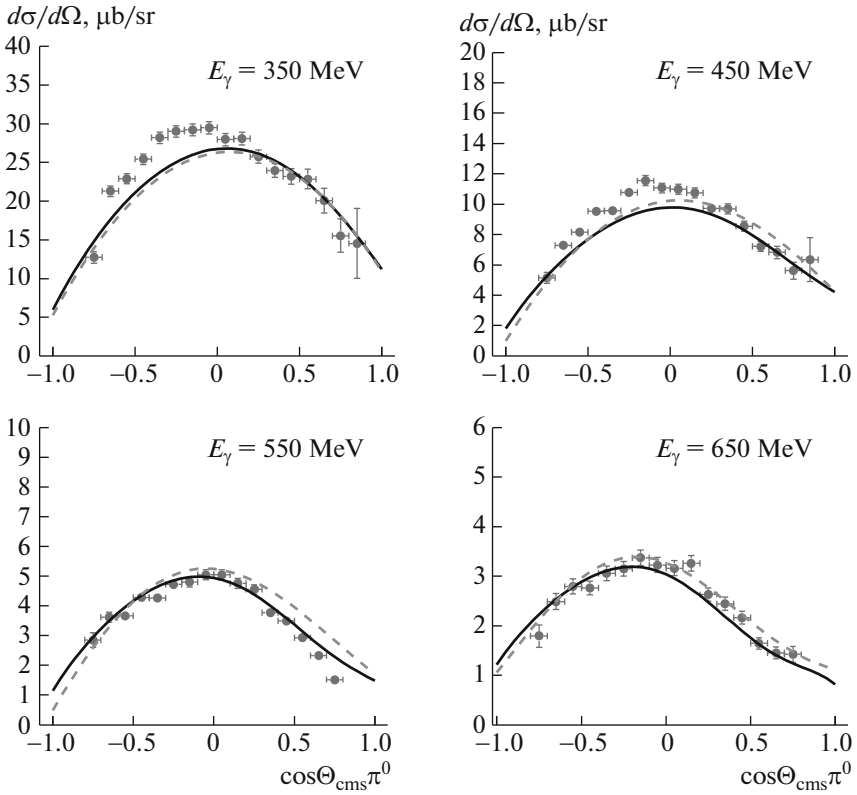

Fig. 5. Obtained $\gamma n \to \pi^0 n$ differential cross section as a function of the cosine of the π^0 emission angle in cms for different incident-photon energies. Our preliminary measurements are depicted by points with error bars. The SAID and MAID theoretical predictions are shown by the solid and dashed curves, respectively.

where M_{a1} is the contribution of the leading IA diagram with a fast neutron, and Δ is the correction including the *pn*-FSI contribution M_b and that of the IA diagram with swapped nucleons, M_{a2} (see Fig. 2). When analyzing the experimental data on the reaction $\gamma d \to \pi^0 np$, the latter correction is taken into account by assigning each event the weight

$$R = \overline{|M_{a1}|^2}/\overline{|M|^2}, \quad (2)$$

where $\overline{|M_{a1}|^2}$ and $\overline{|M|^2}$ are the spin-averaged squared amplitudes computed for the kinematics of a given event. In further event processing, the reaction mechanism is assumed to be determined by the diagram M_{a1}.

It should be noted that the FSI effect plays an important role when analyzing the differential cross section of the discussed reaction, for soft incident photons in particular. The computed differential cross section as a function of the cosine of the π^0 emission angle in the cms is shown in Fig. 3 for incident-photon energies of 300 and 600 MeV. For the beam energy of 300 MeV, the effects of final-state interactions are seen to be significant and should be taken into account in the data analysis.

The results of our preliminary measurements of the $\gamma n \to \pi^0 n$ total cross section performed over the photon-energy range between 180 and 800 MeV with a 10-MeV step in energy are shown in Fig. 4. The relative error of the measured cross section varies between 1.5% and 3%. Our measurements agree with the results of the SAID and MAID [12] partial-wave analyses. The data are better reproduced by the MAID prediction, which takes into account the contributions of high-momentum resonances.

Our preliminary results on the $\gamma n \to \pi^0 n$ differential cross section are shown in Fig. 5 for four values of the incident-photon energy. These are compared with the results of the SAID and MAID analyses. Note that analyzing the data for low energies of incident photons is a challenging task: significant uncertainties may arise from the neutron detection efficiency, which decreases with neutron momentum, reaching only a few percent for these data.

5. CONCLUSIONS

Using the photoproduction data of the A2 collaboration, preliminary measurements of the $\gamma n \to \pi^0 n$ total and differential cross sections were carried out. The analyzed data were obtained using tagged photons with energies between 180 and 800 MeV incident on a deuterium target. The cross sections of neutral-pion photoproduction on a neutron target were obtained using a model formalism for the photon–deuterium collisions based on the SAID parametrization of the $\gamma N \to \pi N$ amplitudes and assuming an s-wave NN final-state interaction. On the whole, the obtained cross sections of the $\gamma n \to \pi^0 n$ reaction agree with the results of the SAID and MAID partial-wave analyses. However, the measured differential cross sections for low tagged-photon energies deviate from theoretical predictions and this calls for performing a more detailed analysis.

ACKNOWLEDGMENTS

We thank the members of the A2 collaboration and the technical staff for their contributions to the measurements. This work was supported in part by the Russian Foundation for Basic Research under grant no. 16-02-00767-a and by the DOE under grants nos. DE-SC0014133 and DE-SC0016583.

REFERENCES

1. I. I. Strakovsky et al., AIP Conf. Proc. **1735**, 040002 (2016).
2. P. Adlarson et al., Phys. Rev. C **92**, 024617 (2015).
3. J. M. Laget, Phys. Rep. **69**, 1 (1981).
4. M. I. Levchuk et al., Phys. Rev. C **74**, 014004 (2006); Phys. Rev. C **82**, 044002 (2010); A. Fix and H. Arenhovel, Phys. Rev. C **72**, 064004 (2005); Phys. Rev. C **72**, 064005 (2005).
5. V. E. Tarasov et al., Phys. Rev. C **84**, 035203 (2011); Phys. At. Nucl. **79**, 216 (2016).
6. Y. Chan et al., IEEE Trans. Nucl. Sci. **25**, 333 (1978).
7. K.-H. Kaiser et al., Nucl. Instrum. Methods Phys. Res. A **593**, 159 (2008).
8. D. Watts, in *Calorimetry in Particle Physics, Proceedings of the 11th Internatinal Conference, Perugia, Italy 2004* (World Scientific, Singapore, 2005), p. 165.
9. M. Martemianov et al., J. Instrum. **10**, T04001 (2015).
10. W. J. Briscoe, I. I. Strakovsky, and R. L. Workman, Inst. of Nucl. Studies of the GWU Database. http://gwdac.phys.gwu.edu/analysis/pr_analysis.html.
11. R. Machleidt et al., Phys. Rep. **149**, 1 (1987).
12. D. Drechsel, S. S. Kamalov, and L. Tiator, Eur. Phys. J. A **34**, 69 (2007).

Translated by A. Asratyan